Supplementary Information

Medium Matters: Modeling the Luminescence Spectra and Emission Decay of $LaPO_4:Eu^{3+}$ Nanoparticles

Daiwen Xiao, Ka-Leung Wong and Peter A. Tanner**

Department of Applied Biology and Chemical Technology, The Hong Kong Polytechnic University, Hung Hom. Kowloon. Hong Kong S.A.R., P.R. China

Table of Contents

S1. Materials, Syntheses and Instrumentation

S1A. Chemicals for NPs. $LaCl_3 \cdot 7H_2O$ (99.999%, Sigma), $EuCl_3 \cdot 6H_2O$ (99.99%, Sigma), methanol (97%, Dieckman), tributyl phosphate (99%, Dieckman), diphenyl ether (99%, Sigma), tridodecylamine (95%, Macklin), phosphoric acid (85 wt % in H_2O, 99.99%, Sigma), dihexyl ether (98%, Macklin).

Chemicals for glass matrices.

B_2O_3 (99.9%, Aladdin), TeO_2 (99.99%, Macklin), $BaCO_3$ (99.95%, Aladdin), Na_2CO_3 (99.99%, Aladdin), CaO (99.5%, Macklin), TiO_2 (99.99%, Aladdin), P_2O_5 (99.995%, Macklin), ZnO (99.99%, Macklin), PbO (99.999%, Macklin), Al_2O_3 (99.997%, Alfa Aesar).

Table S1. Alcohols: RI and supplier

Solvent	Refractive index	Supplier
Propanol	1.3788	Sigma
Butanol	1.4015	Sigma
Pentanol	1.4090	Sigma
Hexanol	1.4178	Sigma
Heptanol	1.4249	Sigma

S1B. Synthesis of NPs:[1,2] A clear solution of 1 mmol lanthanide chloride ($LaCl_3 \cdot 7H_2O$), $EuCl_3 \cdot 6H_2O$ in 1 mL methanol was mixed with 4 mmol tributyl phosphate. Subsequently, the methanol was removed under vacuum at 40 °C in a Schlenk line. Next, 3 mL of diphenyl ether was added, and the water released by the hydrated salts was removed under vacuum at 105 °C. The system was purged with nitrogen in a Schlenk line. After cooling to 50 °C, 3 mmol tridodecylamine was added, followed by 0.7 mL of a 2 M solution of phosphoric acid in dihexyl ether. The reaction mixture was kept for 6 h under nitrogen at 200 °C. After natural cooling, the nanocrystals were precipitated from the reaction mixture by the addition of methanol and washed with methanol three times and then dried by a freeze dryer for 12 h.

S1C. The removal process of surface capping of $LaPO_4$: Eu^{3+} (5 at. %) NPs.[3] The ligands of the $LaPO_4$ nanoparticles were removed using a base-piranha treatment. The piranha solution was prepared by mixing NH_4OH solution (30% in water, heated to 80 °C) and H_2O_2 (30% in water) in an approximate weight ratio of 3:1. The nanoparticles were added to 50 mL of the above solution, and the mixture was left to react at 90 °C for 4 h. After cooling to room temperature, the nanoparticles were collected by centrifugation and washed multiple times with acidic ethanol (ethanol containing 0.1 M HCl, adjusted to pH 4). Finally, the nanoparticles were dried in an oven at 80 °C.

S1D. Solid state sintering synthesis method of $LaPO_4$: Eu^{3+} (0.1 at. %) bulk sample.[4] First, La_2O_3 and Eu_2O_3 were mixed in proportion with $NH_4H_2PO_4$ as starting materials. Then, grinding starting materials in agate mortar with iso-propanol for an hour. Subsequently, the ground product was transferred to a muffle furnace and subjected to heat treatment at 1350°C for 8 h.

S1E. Preparation of glass matrices.[5-10] All the glass matrices were prepared using the traditional melt-quenching method. The composition ratio, melting temperature and time are in the tables (SI, S1H section).

S1F. Preparation of PiG.[8-11] The PiG composites were prepared using a two-step melt-quenching method. In the first step, the tellurite glass matrix with a molar composition (mol%) of $(62\text{-}x)TeO_2$–xB_2O_3–$18ZnO$–$16Na_2O$–$4Al_2O_3$ (x = 0–35) was melted at 800 ℃ for 40 min and then poured onto a copper plate to get the bulk glass matrix. Afterwards, the glass matrix was ground into a fine glass powder by a planetary ball mill (500 rpm min^{-1}, 4 h) for the second melting process. In the second step, the glass powder was put into the corundum crucible and melted at 580 ℃ for 15 min. Then the crucible was taken out from the furnace and the bare $LaPO_4:Eu^{3+}$ (5 at. %) NPs were quickly placed into the high-temperature glass melt with quick stirring by a glass rod for 5 s, and then the melt mixture was immediately poured onto (i) a preheated (280 ℃) copper plate, or (ii) an ice bath, to form the PiG.

With the same two-step melt-quenching method, the second type of PiG was prepared. The tellurite glass matrix TeO_2-ZnO-$BaCO_3$ was melted at 900 ℃ for 30 min and then poured onto a copper plate to get the bulk glass matrix. Afterwards, the glass matrix was ground into a fine glass powder by a planetary ball mill (500 rpm min^{-1}, 4 h) for the second melting process. In the second step, the glass powder was put into the corundum crucible and melted at 600 ℃ for 15 min. Then the crucible was taken out from the furnace and the bare $LaPO_4:Eu^{3+}$ (5 at. %) NPs were quickly poured into the high-temperature glass melt with quick stirring by a glass rod for 5 s, and then the melt mixture was immediately poured into an ice bath, to form the PiG.

For the third type of PiG, the tellurite glass matrix TeO_2-B_2O_3-$BaCO_3$ was melted at 900 ℃ for 30 min and then poured onto a copper plate to get the bulk glass matrix. Afterwards, the glass matrix was ground into a fine glass powder by a planetary ball mill (500 rpm min^{-1}, 4 h) for the second melting process. In the second step, the glass powder was put into the corundum crucible and melted at 700 ℃ for 15 min. Then the crucible was taken out from the furnace and the bare $LaPO_4:Eu^{3+}$ (5 at. %) NPs were quickly placed into the high-temperature glass melt with quick stirring by a glass rod for 5 s, and then the melt mixture was immediately poured into an ice bath, to form the PiG.

S1G. Instrument description. The X-ray diffraction (XRD) patterns of nanoparticles were collected by a Rigaku Smart Lab 9 kW–Advance instrument using CuKα radiation (λ = 1.5418 Å). The emission and excitation spectral measurements at room temperature were recorded by an Edinburgh FLS1000 spectrometer, using a 450 W xenon lamp as the light source and a PMT-900 detector. The spectral transformations and integrations as well as lifetime decay measurements were performed using the software OriginPro 2021. Integrated emission intensities were measured by transforming to an energy scale taking into account the Jacobian correction.

Lifetime measurements were also performed using the Edinburgh FLS1000 spectrometer, utilizing a μF2 Xenon Flashlamp as the light source. Quantum yields (QY) were measured using the

integrating sphere accessory of the Edinburgh instrument. They were calculated by the instrument software and checked by calculation. Transmission Electron Microscope (TEM) photographs of NPs were measured by the JEM-2100F instrument, a multipurpose 200 Kev FE (field emission) analytical electron microscope. Scanning Electron Microscope (SEM) photographs and Element Mapping were collected by the TESCAN VEGA3 instrument with a tungsten thermionic emission SEM system.

S1H. Composition of glasses

Table S2. Borate glass matrix, B_2O_3-BaO.[5]

$\%B_2O_3$	%BaO	Refractive index	Density (g cm^{-3})	Melting temp/time
80	20	1.5592	2.8	1200 °C/30 min
75	25	1.5829	3.07	
70	30	1.6099	3.35	
65	35	1.6270	3.57	
60	40	1.6409	3.76	

Table S3. Borate glass matrix, B_2O_3-TeO_2-Na_2O-CaO-TiO_2.[6]

$\%B_2O_3$	$\%TeO_2$	$\%Na_2O$	%CaO	$\%TiO_2$	Refractive index	Density (g cm^{-3})	Melting temp/time
60	20	10	10	0	2.42	2.912	1000 °C/30 min
60	20	10	9.5	0.5	2.47	2.920	
60	20	10	9	1	2.51	2.998	
60	20	10	8	2	2.56	2.870	
60	20	10	7	3	2.59	2.873	

Table S4. Phosphate glass matrix, P_2O_5-ZnO-PbO.[7]

$\%P_2O_5$	%ZnO	%PbO	Refractive index	Density (g cm^{-3})	Melting temp/time
60	10	30	1.58	3.74	1050 °C/30 min
40	50	10	1.62	3.55	
50	0	50	1.64	4.64	
50	10	40	1.66	4.31	
40	10	50	1.72	5.10	
45	5	50	1.77	4.86	
40	0	60	1.81	5.37	
30	20	50	1.87	5.60	

Table S5. Tellurite glass matrix for PiG, TeO_2-B_2O_3-ZnO-Na_2O-Al_2O_3.[8]

%TeO_2	%B_2O_3	%ZnO	%Na_2O	%Al_2O_3	Refractive index	Density (g cm^{-3})	Melting temp/time
27	35	18	16	4	1.61	3.61	800 °C/30 min
34	28	18	16	4	1.64	3.75	
41	21	18	16	4	1.69	4.03	
48	14	18	16	4	1.76	4.25	
55	7	18	16	4	1.83	4.49	
62	0	18	16	4	1.87	4.79	

Table S6. Tellurite glass matrix for PiG, TeO_2-ZnO-BaO.[9]

%TeO_2	%ZnO	%BaO	Refractive index	Density (g cm^{-3})	Melting temp/time
52.5	22.5	25	1.906	5.30	900 °C/30 min
55	25	20	1.928	5.34	
60	15	25	1.947	5.35	
60	25	15	1.972	5.39	
60	35	5	1.991	5.40	
70	5	25	2.001	5.44	
70	25	5	2.045	5.45	
80	15	5	2.092	5.50	

Table S7. Tellurite glass matrix for PiG, TeO_2-B_2O_3-BaO.[10]

%TeO_2	%B_2O_3	%BaO	Refractive index	Density (g cm^{-3})	Melting temp/time
20	40	40	1.83	4.17	900 °C/30 min
30	35	35	1.84	4.21	
40	30	30	1.92	4.33	
50	25	25	1.93	4.37	
60	20	20	1.98	4.54	
70	15	15	2.02	4.86	

Table S8. Some previous RT measurements of lifetime of $LaPO_4$ doped with Eu^{3+}.

System	**$^5D_0$ Lifetime (ms)**	**Ref.**
1.5 µm $LaPO_4$:Eu^{3+} (5 at.%) microspheres	2.41	12
bulk $LaPO_4$:Eu^{3+} (2 at.%)	3.18	13
4 nm $LaPO_4$:Eu^{3+} (5 at.%) NPs	3.9	14
15.7 nm $LaPO_4$:Eu^{3+} (5 at.%) NPs	0.97	15
particles >100 nm $LaPO_4$:Eu^{3+} (10 at.%)	3.31	16
5 nm $LaPO_4$:Eu^{3+} (10 at.%) NPs	2.44	16

10-20 nm $LaPO_4:Eu^{3+}$ (4.2 at.%) NPs	2.25	17
5-10 nm $LaPO_4:Eu^{3+}$ (10%) nanorods	4.65, 1.75	18

S2. Theoretical background

The models of local field effects are usually based upon cavities although Aspnes[19] and others[20,21] have deduced the same equations without reference to those. The Lorentz (Full Cavity or Virtual Cavity) model is employed for bulk materials.[22-24]

The spontaneous emission rate (A s^{-1}) for the ED allowed transition between upper state A and lower state B in an isotropic medium of refractive index n is given by:[22]

$$A = A(0)n\Gamma \quad \text{(S1)}$$

where $A(0)$ is the rate in a (vacuum) medium of refractive index equal to one, and Γ (the local field correction, dimensionless) represents the ratio of the local to the macroscopic electric field experienced by the chromophore $(E_{loc}/E_{macr})^2$. The radiative lifetime τ is the reciprocal of the spontaneous emission rate A. The intensity of this transition (in photon counts s^{-1}) is given by:

$$I_{AB} = N_A A \quad \text{(S2)}$$

For MD allowed transitions, where the magnetic susceptibility equals the vacuum value, since the microscopic magnetic field operator has no refractive index dependence, the variation of spontaneous emission rate just varies approximately as the cube of the photon density of states, that is, to the cube of the refractive index of the medium. Considering this effect, for our bulk samples:

$$A_{MD,bulk} = A_{MD}(0)n_{cr}^3 \quad \text{(S3)}$$

where 14.65 s^{-1} has been given for the value of $A_{MD}(0)$ for the $^5D_0 \rightarrow {}^7F_1$ transition of Eu^{3+},[25,26] and the refractive index of $LaPO_4$ is n_{cr} = 1.79. This includes the assumption that the ED contribution to the $^5D_0 \rightarrow {}^7F_1$ transition is negligible.

The use of an effective refractive index is taken to be valid when the size of the particles is much smaller than the wavelength of radiation. In the present case the effective refractive index is defined for a Maxwell-Garnett nanocomposite: i.e., the medium (with refractive index n_{med}) in which the nanoparticles (with refractive index n_{np}) are embedded:[27]

$$n_{eff}^2 = n_{med}^2 \left\{ \frac{2f(n_{np}^2 - n_{med}^2) + n_{np}^2 + 2n_{med}^2}{2n_{med}^2 + n_{np}^2 - f(n_{np}^2 - n_{med}^2)} \right\} \quad \text{(S4)}$$

where f is the filling factor (i.e., volume ratio of the space occupied by the particles). Otherwise, the effective refractive index has been defined:[28]

$$n'_{eff} = f \cdot n_{np} + (1 - f) \cdot n_{med} \quad \text{(S5)}$$

As shown in Fig. S1, the values of n_{eff} and n_{med} become closer together when n_{med} approaches the same value as n_{np} (1.79 in this case). The Eq. S4 and S5 give similar values of n_{eff} except at higher values of f.

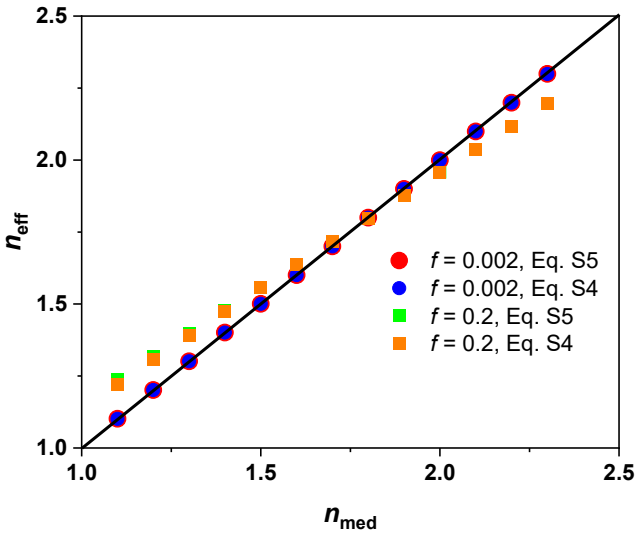

Figure S1. Variation of n_{eff} with n_{med} according to Eqs. (S4) and (S5), with two different values of filling factor, f: 0.002 and 0.2.

Pukhov *et al.*[29-31] considered the spontaneous emission rates for nanoparticles of various geometries embedded in media. The model is valid only for small-sized optical centers in a crystalline nanoparticles that have a spherical shape, with linear sizes much less than the wavelength of spontaneous emission and suspended in a non-absorbing dielectric medium. Other assumptions are given in the manuscript of Pukhov *et al.*[30] The f =1 system, the bare NPs, have been included in the model. For simplicity, we assume spherical NPs. Analogous to Eq. (S3), for the case of MD spontaneous emission of NPs:[31]

$$A_{\mathrm{MD,np}} = A_{\mathrm{MD}}(0) n_{\mathrm{eff}}^3 \quad \text{(S6a)}$$

$$A_{\mathrm{MD,np}} = A_{\mathrm{MD,bulk}} n_{\mathrm{eff}}^3 / n_{\mathrm{np}}^3 \quad \text{(S6b)}$$

and $$1/(\tau_{\mathrm{meas,MD,np}}) = A_{\mathrm{MD,np}} + k'_{\mathrm{nr}} \quad \text{(S6c)}$$

where $1/(\tau_{\mathrm{meas,MD,np}})$ is the MD contribution to the experimentally measured rate constant and k'_{nr} is the corresponding nonradiative rate contribution.

As a function of effective refractive index, the ED spontaneous emission rate is given by:

$$A_{\mathrm{ED,np}} = A_{\mathrm{ED,bulk}} \times \frac{n_{\mathrm{eff}}}{n_{\mathrm{np}}} \left\{ \frac{3}{\left(\frac{n_{\mathrm{np}}^2}{n_{\mathrm{med}}^2}\right) + 2 - f\left[\left(\frac{n_{\mathrm{np}}^2}{n_{\mathrm{med}}^2}\right) - 1\right]} \right\}^2 \quad \text{(S7a†)}$$

where $A_{\mathrm{ED,bulk}}$ refers to the bulk material. The reciprocal of the measured lifetime, $(1/\tau_{\mathrm{meas,np}})$, can be written as:

$$1/(\tau_{\mathrm{meas,np}}) = A_{\mathrm{ED,np}} + A_{\mathrm{MD,np}} + k_{\mathrm{nr}} \quad \text{(S7a)}$$

and k_{nr} is the average nonradiative rate contribution. Here, $A_{\mathrm{ED,np}}$ is given by Eq. (S7a) and $A_{\mathrm{MD,np}}$ can be given as either Eq. (S6a) or (S6b) and here it is in the former:

$$1/(\tau_{\mathrm{meas,np}}) = A_{\mathrm{ED}}(0) \times n_{\mathrm{eff}} \left\{ \frac{3n_{\mathrm{med}}^2}{n_{\mathrm{np}}^2 + 2n_{\mathrm{med}}^2 - f[n_{\mathrm{np}}^2 - n_{\mathrm{med}}^2]} \right\}^2 + A_{\mathrm{MD}}(0) n_{\mathrm{eff}}^3 + k_{\mathrm{nr}} \quad \text{(S7b)}$$

The variation of ED:MD intensity ratio with refractive index for NPs is obtained by dividing Eq. (S7a) by Eq. (S6b):

$$A_{\mathrm{ED,np}} : A_{\mathrm{MD,np}} = \frac{A_{\mathrm{ED,bulk}}}{A_{\mathrm{MD,bulk}}} \left\{ \frac{9n_{\mathrm{med}}^2 n_{\mathrm{np}}^2}{2n_{\mathrm{med}}^2 + n_{\mathrm{np}}^2 - f(n_{\mathrm{np}}^2 - n_{\mathrm{med}}^2)} \right\} \left\{ \frac{1}{2f(n_{\mathrm{np}}^2 - n_{\mathrm{med}}^2) + n_{\mathrm{np}}^2 + 2n_{\mathrm{med}}^2} \right\} \quad \text{(S8a)}$$

$$= \frac{A_{\mathrm{ED}}(0)}{A_{\mathrm{MD}}(0)} \left\{ \frac{9n_{\mathrm{med}}^2}{2n_{\mathrm{med}}^2 + n_{\mathrm{np}}^2 - f(n_{\mathrm{np}}^2 - n_{\mathrm{med}}^2)} \right\} \left\{ \frac{1}{2f(n_{\mathrm{np}}^2 - n_{\mathrm{med}}^2) + n_{\mathrm{np}}^2 + 2n_{\mathrm{med}}^2} \right\} \quad \text{(S8b)}$$

Assuming the appropriate refractive index of $LaPO_4$ ($n_{\mathrm{np}} = 1.79$) and the filling factor of 0.02, Fig. 1f depicts the variation of Eq. (S8b) in this case. The figure shows that from the refractive index range 1.5 to 1.7, the value of the ratio ED:MD is predicted to decrease by 5.4% for NPs.

The model employed in the literature for the correction of spontaneous emission probability for micron size materials in a medium of refractive index n is the Virtual Cavity model. The relevant equation is for electric dipole radiation:

$$\text{Virtual Cavity model: } A(n) = A(0) n \left[\frac{n^2+2}{3} \right]^2 \quad \text{(S9)}$$

Using this model, the reciprocal lifetimes, $k = 1/\tau$, may be fitted as a function of refractive index by the equation:

$$\text{Virtual Cavity model: } k(n) = 14.65n^3 + A(0) n \left[\frac{n^2+2}{3} \right]^2 + k_{nr} \quad \text{(S10)}$$

$$\text{Virtual Cavity model: } ED{:}MD\ ratio = A(0) n \left[\frac{n^2+2}{3} \right]^2 / (14.65n^3) \quad \text{(S11)}$$

For NPs, the index n in Eq. S9-S11 can be replaced by the effective refractive index, n_{eff}.

The fully microscopic model of Crenshaw and Bowden predicts a weaker dependence of radiative lifetime upon the medium refractive index:[32-34]

$$A(n) = A(0) \left[\frac{n^2+2}{3} \right] \quad \text{(S12)}$$

So that the reciprocal lifetime is given by:

$$k(n) = 14.65n^3 + A(0) \left[\frac{n^2+2}{3} \right] + k_{nr} \quad \text{(S13)}$$

And the ED:MD ratio by:

$$ED{:}\,MD\ ratio = A(0)\left[\frac{n^2+2}{3}\right]/(14.65n^3) \quad \text{(S14)}$$

As above, for NPs, the index n in Eq. S12-S14 can be replaced by the effective refractive index, n_{eff}.

This model does not provide good fits to our experimental data and is not further considered.

In the above formulae, which value of $n(\lambda)$ should we plug into the formula: (i) n at the absorption wavelength? (ii) n at the emission wavelength? (iii) an average over the entire emission spectrum, or individual values at different wavelengths? Ideally, the answer is (ii). Due to the lack of data and the procedure adopted in previous studies of the local field effect, we have made the assumption that the refractive index change can be neglected over the range of emission wavelengths. Hence, for Eu^{3+} the choice adopted is the refractive index at the fundamental transition energy of the ion in the particular host. Using a single n value is a good approximation because the dispersion of n is often small across the visible range and the error involved is comparable with that of other assumptions in the calculation.

Some data fits were carried out assuming various assumptions of the refractive index dependence of the parameter k_{nr}. It was found that slightly improved results could be achieved by using a dependence upon the dielectric constant (i.e. upon n^2) or using a real cavity type dependence. We have not included these results because they only serve as complications.

S3. Nanocavity model for $LaPO_4:Eu^{3+}$ NPs

The nanocrystal-cavity (nanocavity) model has been employed in several publications describing the optical behavior of $LaPO_4:Eu^{3+}$ NPs.[35,36] The model is the same as the Real Cavity model except that the quantity 1^2 in the denominator is replaced by n_{np}^2. The same model has been employed by Yablonovich *et al.* [37] and Chew.[38]

The equation for the decay rate for an electric dipole transition in a refractive index n_{med} according to the Nanocrystal Cavity model (Nanocavity model) is given in Ref. 35, Eq. 5; Ref. 36, Eq. 2 as:

$$A_{\text{ED,NP}} = A_{\text{ED}}(0)n_{\text{med}}\left(\frac{3n_{\text{med}}^2}{2n_{\text{med}}^2+n_{\text{np}}^2}\right)^2 \quad \text{(S15)}$$

In the manuscript, we have:

$$A_{\text{ED,NP}} = A_{\text{ED,bulk}} \times \frac{n_{\text{eff}}}{n_{\text{np}}}\left\{\frac{3}{\left(\frac{n_{\text{np}}^2}{n_{\text{med}}^2}\right)+2-f\left[\left(\frac{n_{\text{np}}^2}{n_{\text{med}}^2}\right)-1\right]}\right\}^2 \quad \text{(S7a)}$$

When $f = 0$, $n_{\text{eff}} = n_{\text{med}}$, so this becomes:

$$A_{\mathrm{ED,NP}} = A_{\mathrm{ED,bulk}} \times \frac{n_{\mathrm{med}}}{n_{\mathrm{np}}} \left\{ \frac{3}{\left(\frac{n_{\mathrm{np}}^2}{n_{\mathrm{med}}^2}\right)+2} \right\}^2 = A_{\mathrm{ED,bulk}} \times \frac{n_{\mathrm{med}}}{n_{\mathrm{np}}} \left\{ \frac{3n_{\mathrm{med}}^2}{n_{\mathrm{np}}^2+2n_{\mathrm{med}}^2} \right\}^2 \quad \text{(S16)}$$

assuming $A_{\mathrm{ED}}(\mathrm{bulk}) = n_{\mathrm{np}} A_{\mathrm{ED}}(0)$ when $f_{\mathrm{L}} = 1$: Ref. 31, Eq. 9; Ref. 30, Eq. 1, we have:

$$A_{\mathrm{ED,NP}} = A_{\mathrm{ED}}(0) \times n_{\mathrm{med}} \left\{ \frac{3n_{\mathrm{med}}^2}{n_{\mathrm{np}}^2+2n_{\mathrm{med}}^2} \right\}^2 \quad \text{(S15)}$$

Which is the same as the Nanocavity model. Hence, all of the equations employing the model of Pukhov *et al*. in the present work will similarly reduce to the Nanocavity model when $f = 0$ and $n_{\mathrm{eff}} = n_{\mathrm{med}}$.

S4. Fitting of lifetimes of $LaPO_4:Eu^{3+}$ NPs in alcohols

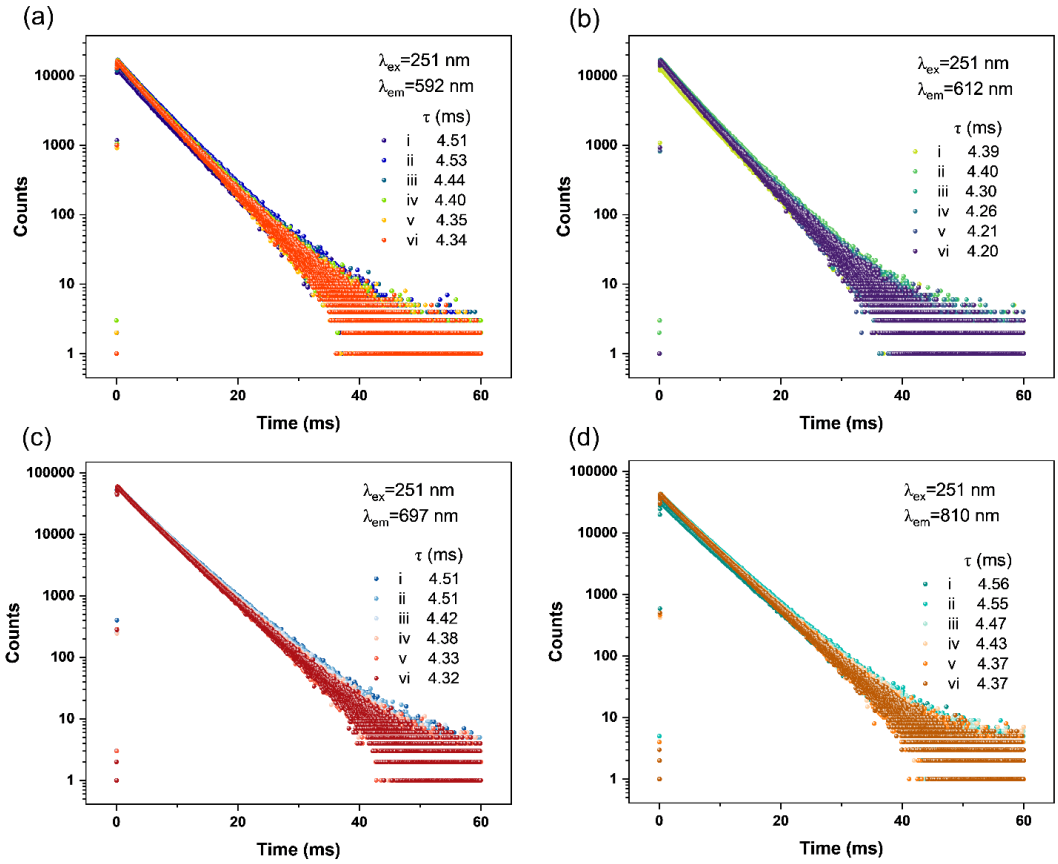

Figure S2. Experimental results for emission decay of $LaPO_4:Eu^{3+}$ (5 at. %) NPs dispersed in different solvents and monitored at (a) 592 nm, (b) 612 nm, (c) 697 nm, (d) 810 nm. i propanol, ii butanol, iii Pentanol, iv hexanol, v heptanol, vi heptanol-1(repeat one).

The emission decays were by monoexponential equations and the resulting lifetimes for $LaPO_4:Eu^{3+}$ NPs dispersed in alcohols have been fitted in Fig. 2h by the model of Pukhov *et al*. [S29-S31] A repeated experiment has also been included in Fig. 2g.

It was found that fitting Figs. 2g and 2h using the simple Virtual Cavity model realized data fits with similar R_{adj}^2 values as from the model of Pukhov *et al*. The fitted parameters k_{nr} were generally similar but the values of $A_{ED}(0)$ were about 2.75 times smaller for the Virtual Cavity model. With extrapolation to n = 1, this means that the QY are predicted to be much smaller for this model (Table S6).

Table S9. Comparison of fits to lifetimes of NPs dispersed in alcohols.

λ_{em} (nm)	Eq. S10 R_{adj}^2	Eq. S7b R_{adj}^2	Eq. S10 $A_{ED}(0)$, k_{nr} (s^{-1})	Eq. S7b $A_{ED}(0)$, k_{nr} (s^{-1})
2nd batch				
697	0.96017	0.96068	55,48	152,36
809	0.96934	0.96993	52,50	145,41
592	0.96224	0.96301	56,43	156,31
612	0.95202	0.95277	61,38	170,25
1st batch				
697	0.95106	0.94799	51,82	140,74
592	0.93538	0.9323	49,95	132,87
612	0.91935	0.91594	53,124	145,115
Average Values	Eq. S10 $A_{ED}(0)$, k_{nr} (s^{-1})	Eq. S7b $A_{ED,bulk}$, k_{nr} (s^{-1})	Eq. S7b $A_{ED}(0)$, k_{nr} (s^{-1})	QY%, n=1 Eq. S10, Eq. S7b
2nd batch	56(4), 45(5)	279(19), 33(7)	156(11), 33(7)	48, 76
1st batch	51(2), 100(22)	249(11), 92(21)	139(6), 92(21)	31, 57

Eq. S10 is the Virtual Cavity model; Eq, S7b is the model of Pukhov *et al*. R_{adj}^2 is the adjusted coefficient of determination in the fits; there are two free parameters in each case. The percentage quantum yield, QY%, refers to the situation of n = 1: where $1/\tau = 14.65+A_{ED}(0)+k_{nr}$.

From our studies of different batches of NPs, the fitted values of the parameters $A_{ED,bulk}$ and k_{nr} for NPs from Eq. S7b were found to be in the range of 266±22 s^{-1} and 59±34 s^{-1}, respectively.

The calculated nonradiative rates are fairly similar when using Eq. S10 or S7b. The sum of $A_{ED,bulk}+k_{nr}$ for $LaPO_4:Eu^{3+}$ (5 at.%) micron size particles is in the range of 219-360 s^{-1} from literature values (Table S8); the values calculated using the Real Cavity model of Pukhov (Eq.

7b) and the Virtual Cavity model (Eq. S10) are in the ranges of 313-341 s^{-1} and 145-191 s^{-1}, respectively (Table S9), so that the former model shows better agreement, considering the expected increase in k_{nr} from micron to NPs

S5. Spectra of bare $LaPO_4$: Eu^{3+} (5 at.%) NPs

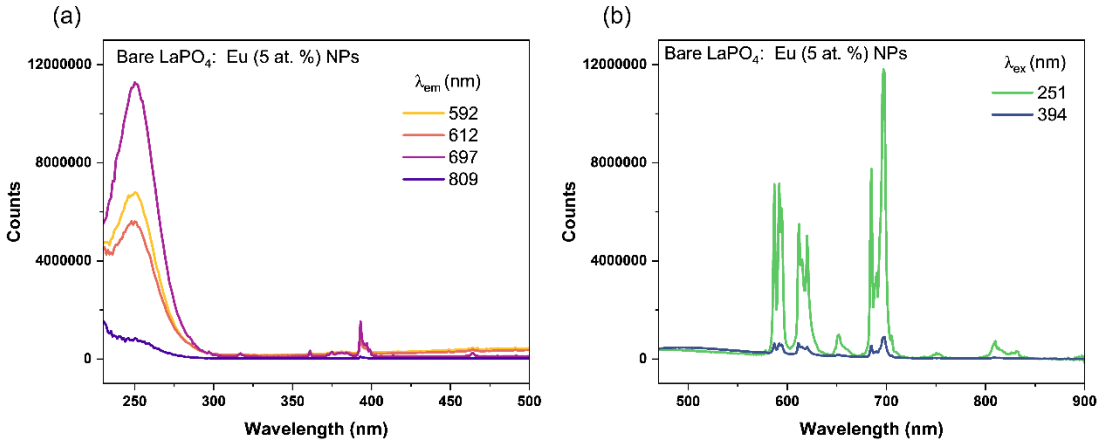

Figure S3. Excitation (a) and emission (b) spectra of bare $LaPO_4$: Eu^{3+} (5 at. %) NPs powder

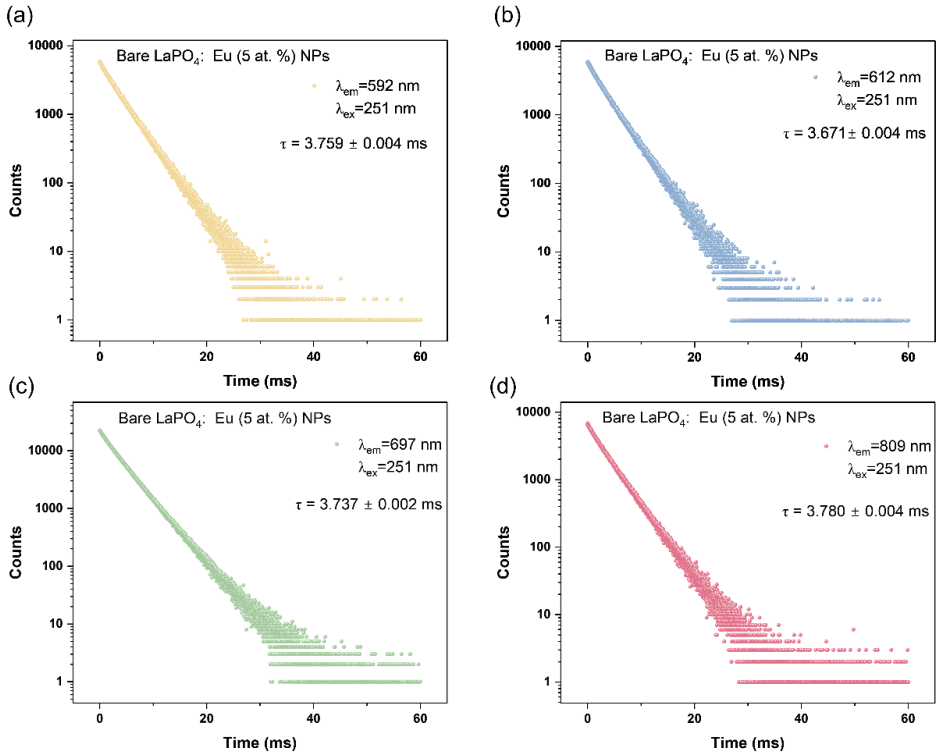

Figure S4. (a-d) Lifetimes of bare $LaPO_4$:Eu^{3+} (5 at. %) NPs, monitoring 592, 612, 697, 809 nm respectively.

S6. Spectra of $LaPO_4$: Eu^{3+} (0.1 at. %) micron size powder

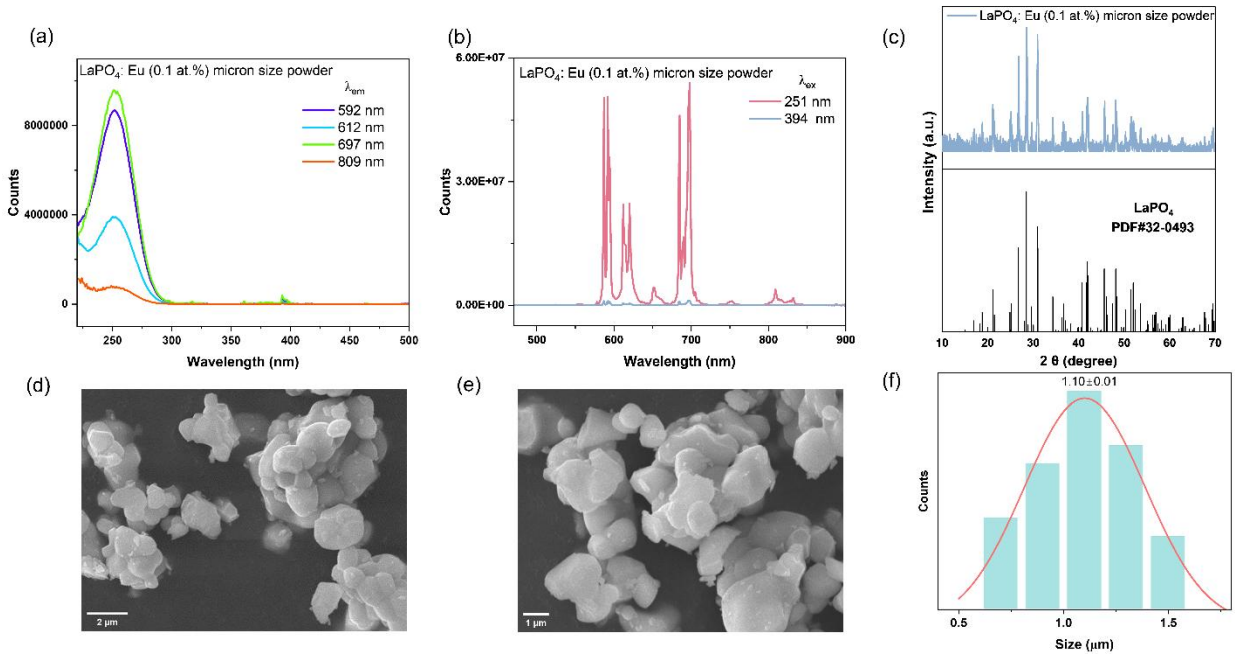

Figure S5. $LaPO_4$:Eu^{3+} (0.1 at. %) micron size powder: (a) Excitation spectra. (b) Emission spectra. (c) X-ray diffractograms. (d), (e) Scanning electron micrographs. (f) Particle size.

S7. Selected spectra of glass matrices

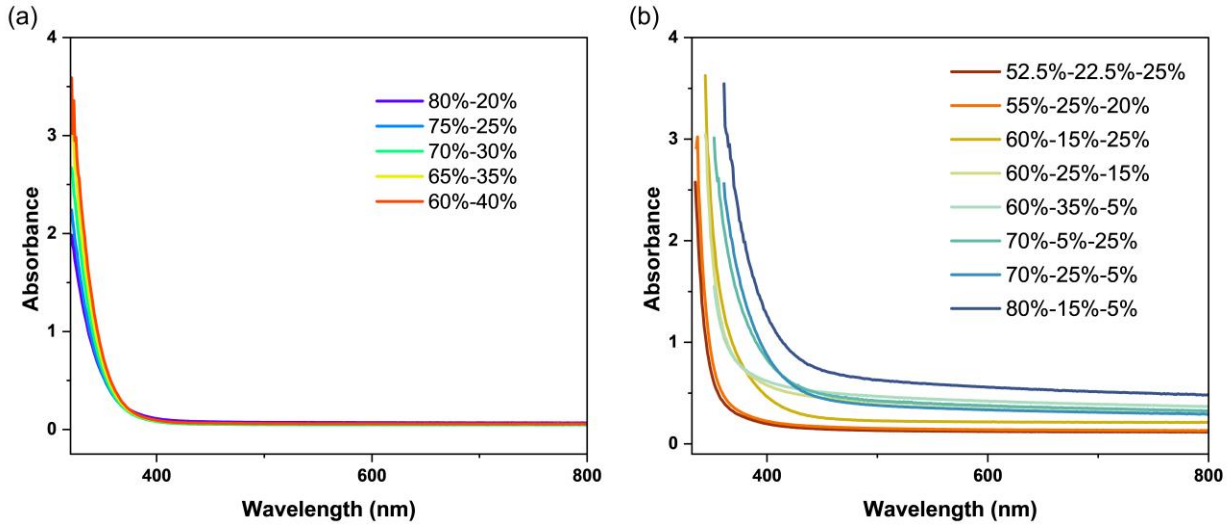

Figure S6. Absorption spectra of (a) prepared x%B_2O_3-y%BaO borate glasses; (b) $a$$TeO_2$-$b$ZnO-$c$BaO glasses.

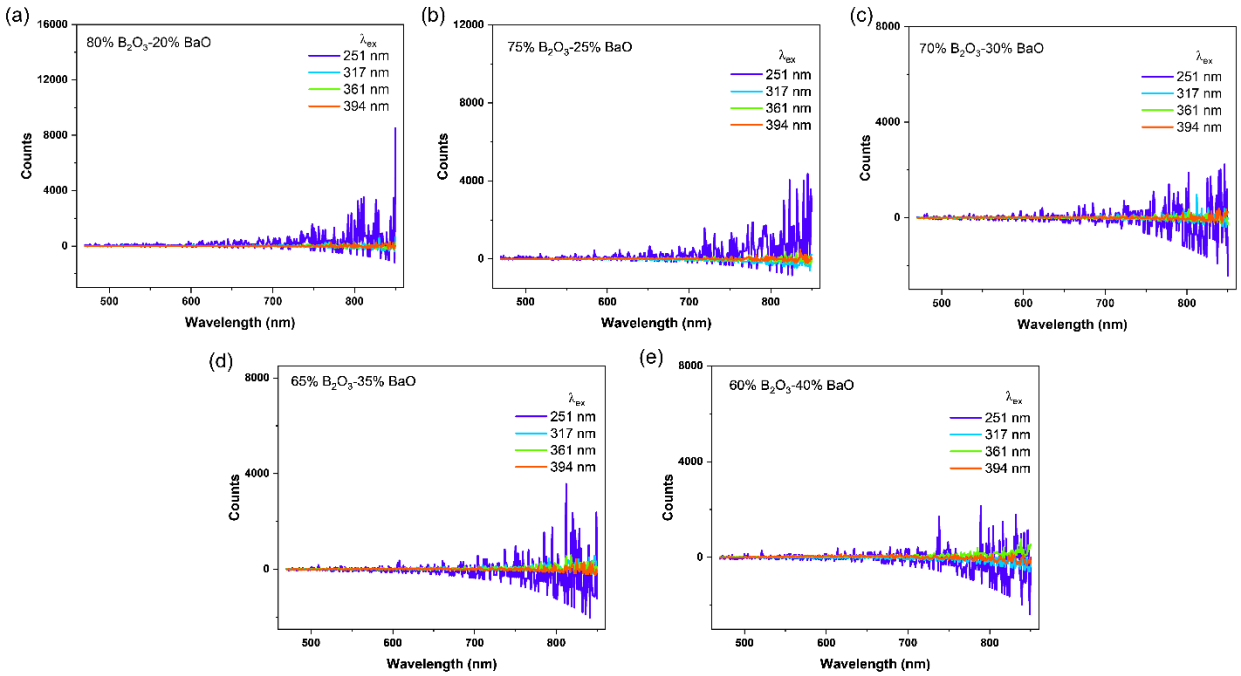

Figure S7. Emission spectra of B_2O_3-BaO borate glass matrices.

S8. Glass powders mixed with NPs

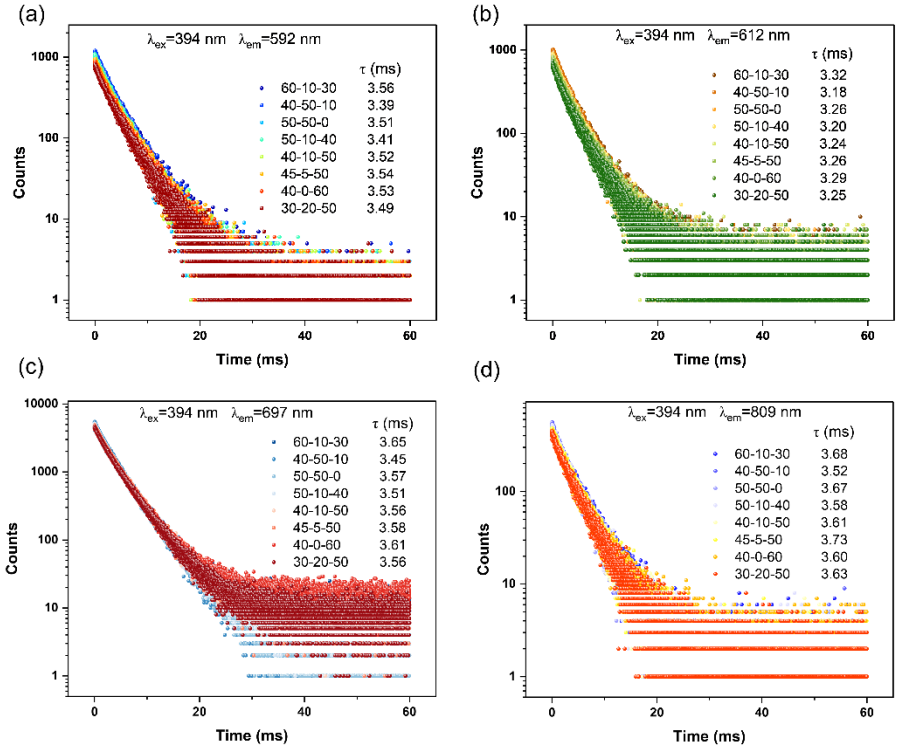

Figure S8. Lifetime of phosphate glasses $a\%P_2O_5$-$b\%$ZnO-$c\%$PbO mixed with NPs powder.

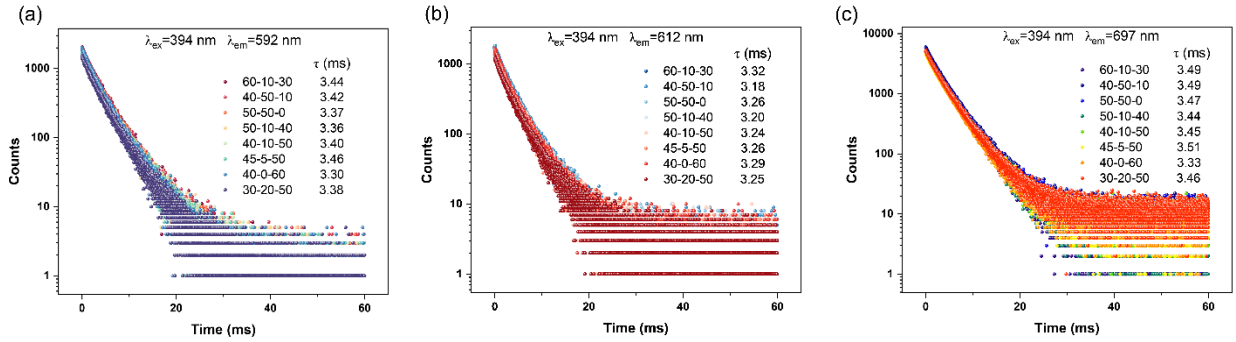

Figure S9. Lifetime of compressed discs made from phosphate glasses $a\%P_2O_5$-$b\%$ZnO-$c\%$PbO mixed with NPs powder.

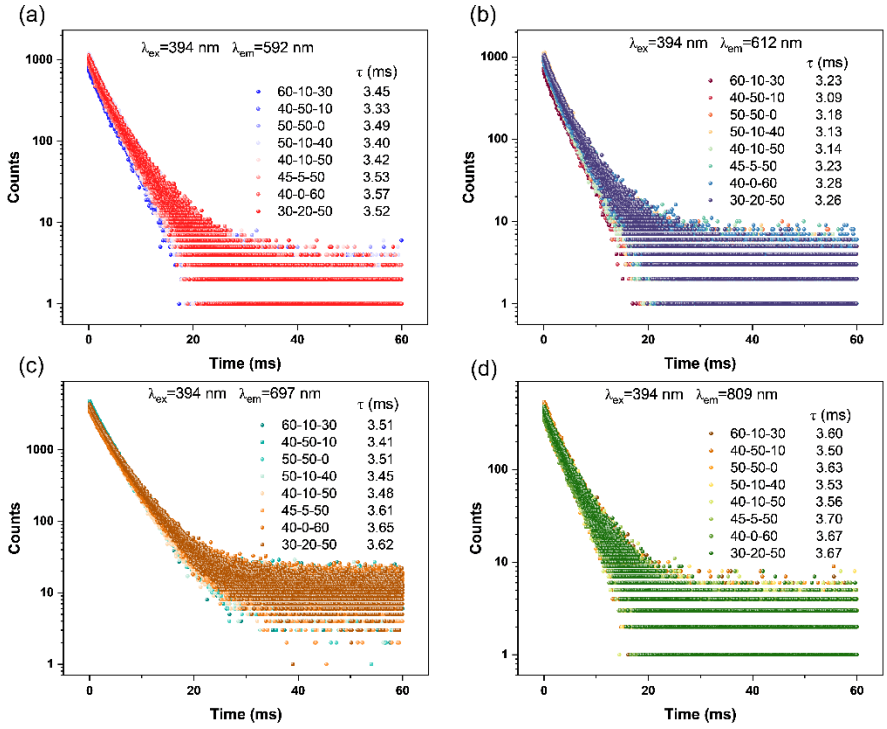

Figure S10. Repeated lifetime of phosphate glasses $a\%P_2O_5$-$b\%$ZnO-$c\%$PbO mixed with NPs powder.

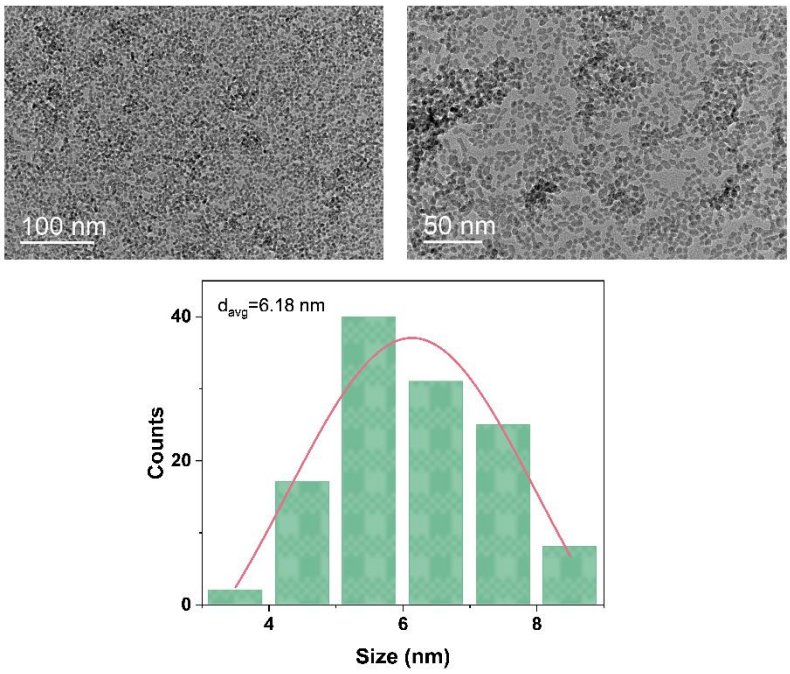

Figure S11. TEM photographs and the size distribution of the NPs dispersed in P_2O_5-ZnO-PbO glasses.

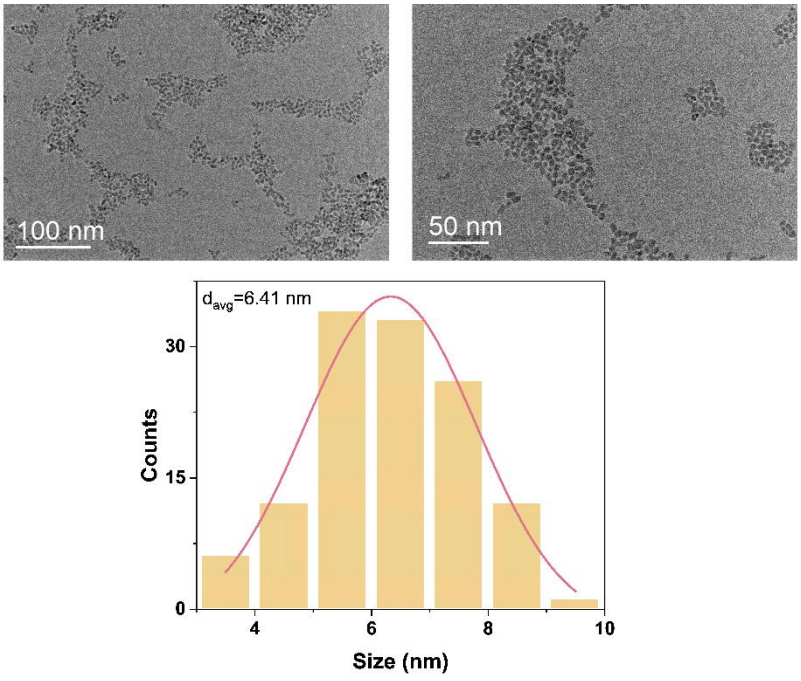

Figure S12. TEM photographs and the size distribution of the NPs dispersed in B_2O_3-TeO_2-Na_2O-CaO-TiO_2 glasses.

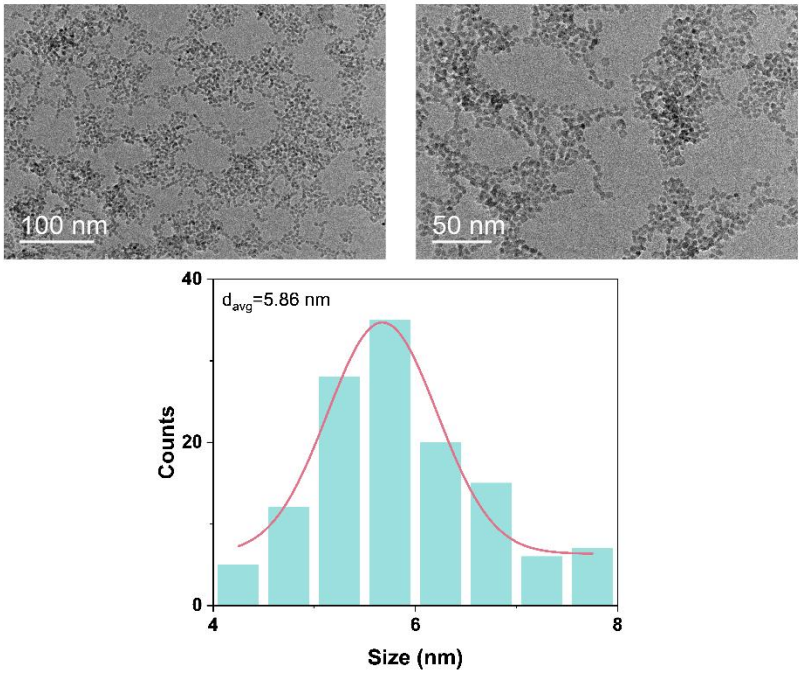

Figure S13. TEM photographs and the size distribution of the NPs dispersed in B_2O_3-TeO_2-Na_2O-CaO-TiO_2 glasses.

S9. Fitting of lifetime data from Ref. 39.

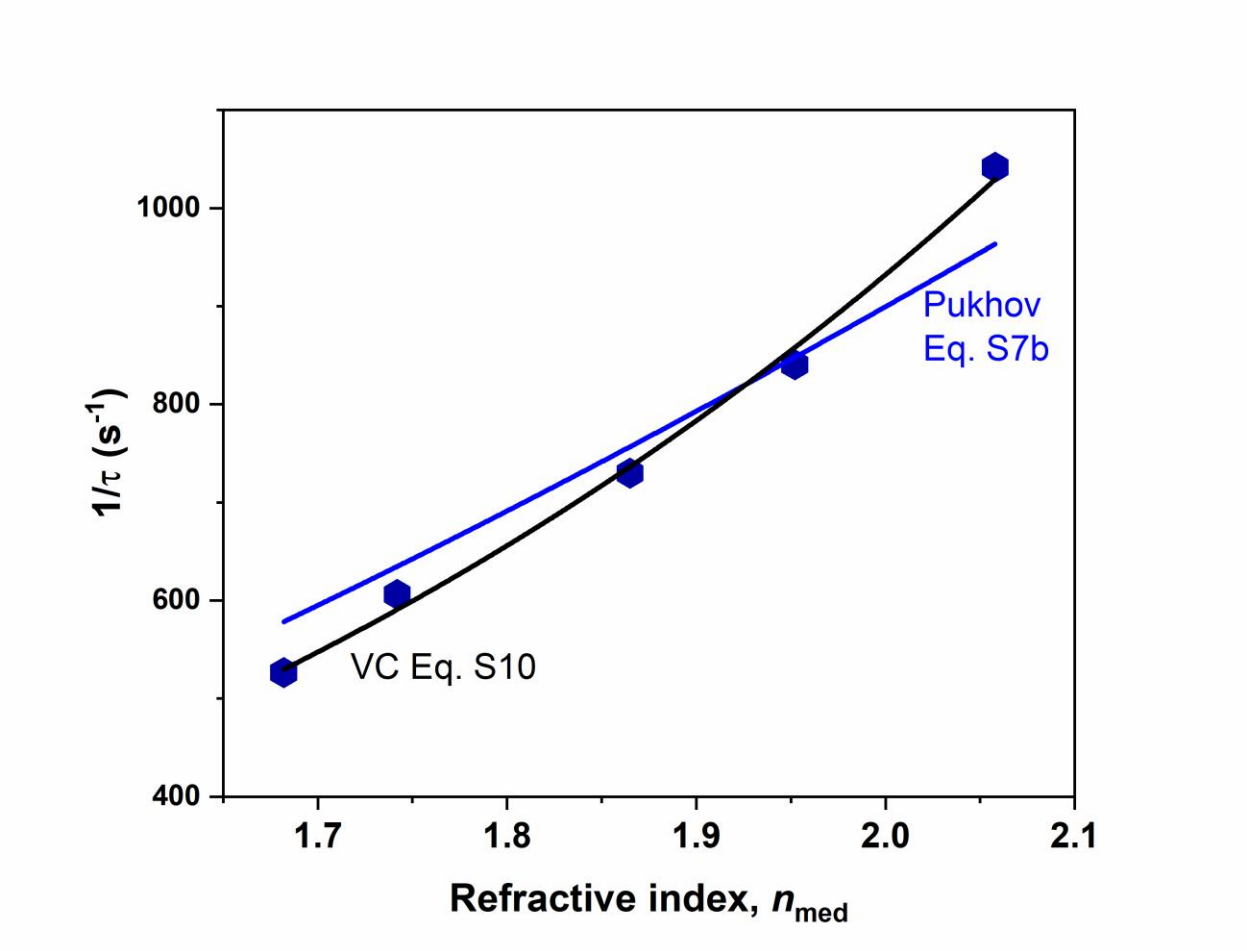

Figure S14. Lifetime data from Ref. 39 for B_2O_3-PbO-Eu_2O_3 glasses fitted by two models.

S10. Comparison with NPs in melted phosphor in glass (PiG)

The spectra and lifetime of $LaPO_4$:Eu (5 at.%) NPs TeO_2-B_2O_3-ZnO-Na_2O-Al_2O_3 PiG melted at 800 ºC and 1000 ºC for 15 min (λ_{exc} = 394 nm) are displayed in Fig. S15 (a), (b) and (c), (d), respectively. The integrity of the $LaPO_4$:Eu^{3+} NP moiety has been lost and Eu^{3+} is now incorporated into the glass framework, as in Fig. 4a. The lifetime becomes shorter.

Figure S15 (e) compares the spectra of bare NPs with the further melted PiG and the 62-0-18-16-4 PiG. The further melted PiG is observed to contribute some intensity to the PiG, as marked by green arrows.

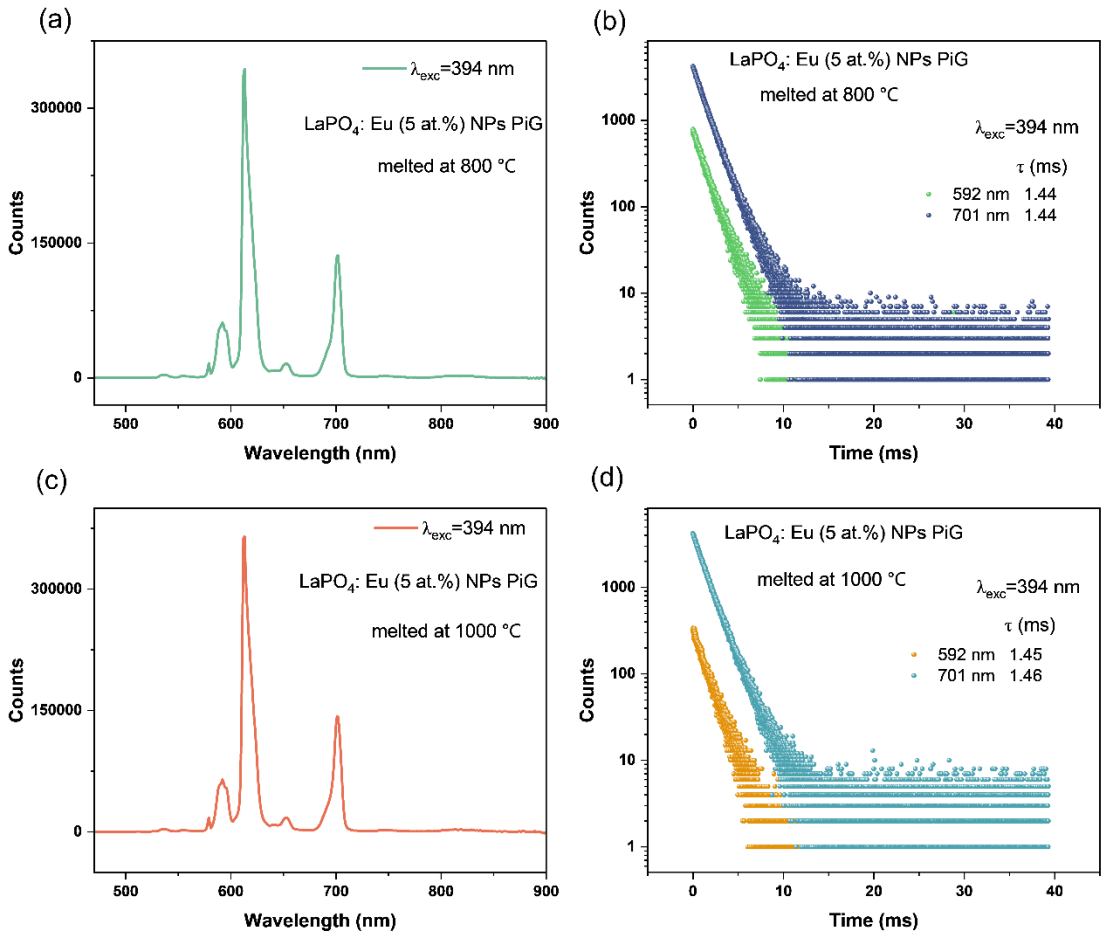
(a)
λexc=394 nm
LaPO4: Eu (5 at.%) NPs PiG
melted at 800 °C
Counts
Wavelength (nm)
(b)
LaPO4: Eu (5 at.%) NPs PiG
melted at 800 °C
λexc=394 nm
τ (ms)
592 nm 1.44
701 nm 1.44
Counts
Time (ms)
(c)
λexc=394 nm
LaPO4: Eu (5 at.%) NPs PiG
melted at 1000 °C
Counts
Wavelength (nm)
(d)
LaPO4: Eu (5 at.%) NPs PiG
melted at 1000 °C
λexc=394 nm
τ (ms)
592 nm 1.45
701 nm 1.46
Counts
Time (ms)

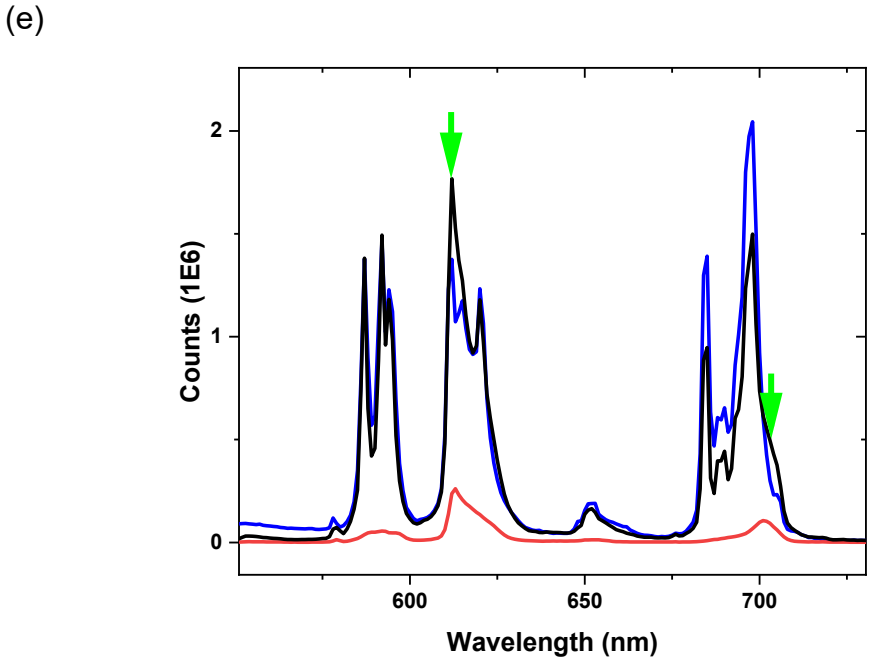
(e)
Counts (1E6)
Wavelength (nm)

Figure S15. The emission spectra and lifetime of $LaPO_4$:Eu (5 at. %) NPs in 41% TeO_2-21% B_2O_3-18% ZnO-16% Na_2O-4% Al_2O_3 PiG melted at 800 °C (a), (b) and 1000 °C (c), (d) for 15 min. (e) Comparison of the spectra normalized on ${}^5D_0 \rightarrow {}^7F_1$ for bare NPs (blue) with 62% TeO_2-0% B_2O_3-18% ZnO-16% Na_2O-4% Al_2O_3 PiG (black). The TeO_2-B_2O_3-ZnO-Na_2O-Al_2O_3 PiG melted at 800 °C is shown in red.

S11. TEM photographs of NPs in phosphor in glass (PiG)

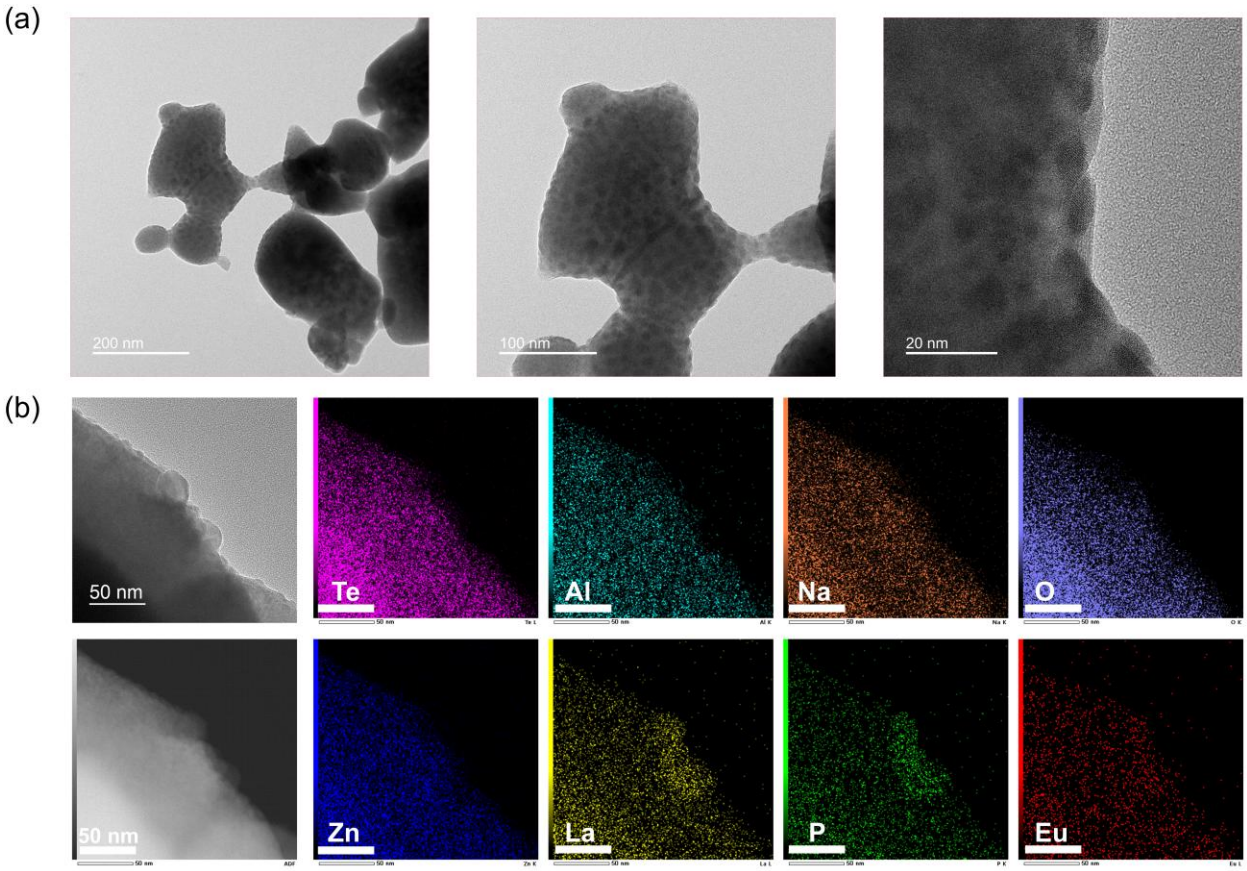

Figure S16. (a)TEM photographs and (b) elemental mapping images of selected *a*%TeO_2-*b*%B_2O_3-*c*%ZnO-*d*%Na_2O-*e*%Al_2O_3 (*a* = 41, *b* = 21, *c* = 18, *d* = 16, *e* = 4) PiG.

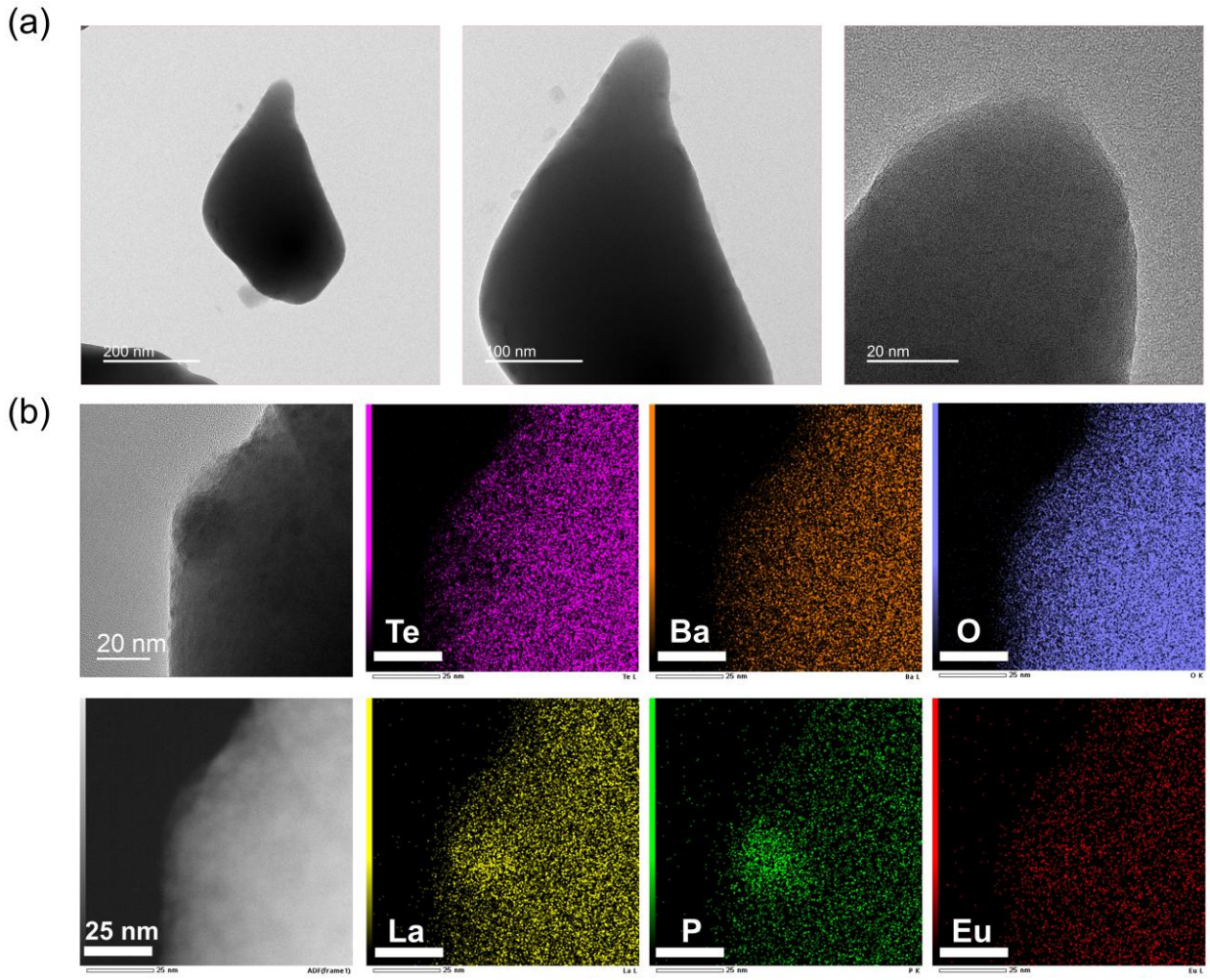

Figure S17. (a)TEM photographs and (b) elemental mapping images of selected *a*%TeO_2-*b*%ZnO-*c*%BaO (*a*=60, *b*=25, *c*=15) PiG.

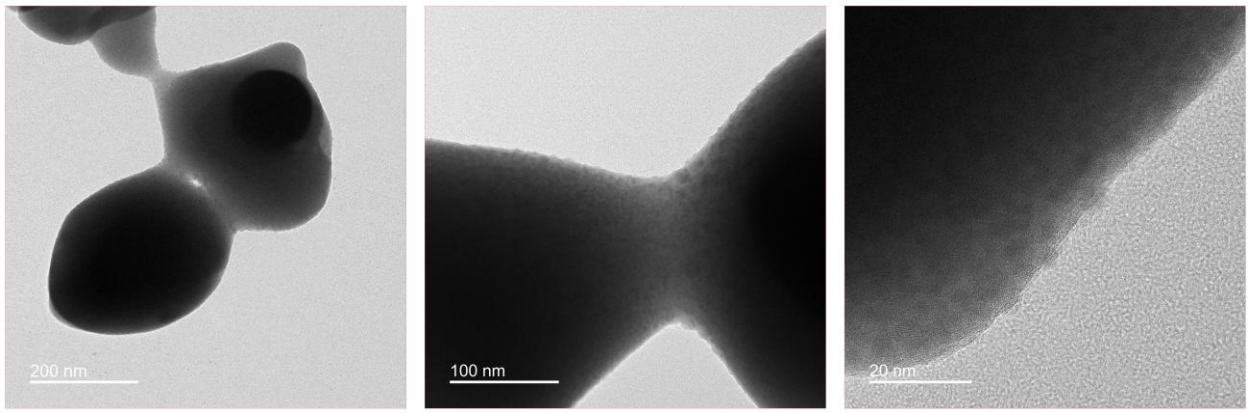

Figure S18. TEM photographs of selected *a*%TeO_2-*b*%BaO-*c*%B_2O_3 (*a* = 50, *b* = 25, *c* = 25) PiG.

S12. ED:MD ratio of NPs in phosphor in glass (PiG)

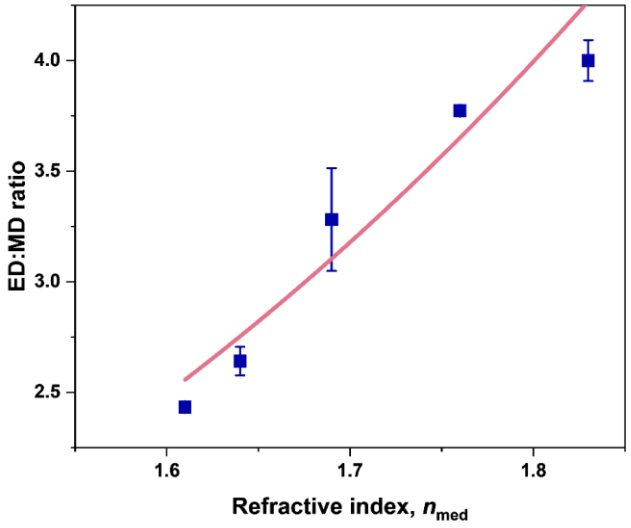

Figure S19. Plot of mean ED:MD ratio in Fig. 5d for TeO_2-B_2O_3-Na_2O-CaO-TiO_2 glasses with the fit: ED:MD ratio = $A \times n_{med}^4$, where A is a constant.

S13. Calculation of quantum yield for NPs in heptanol.

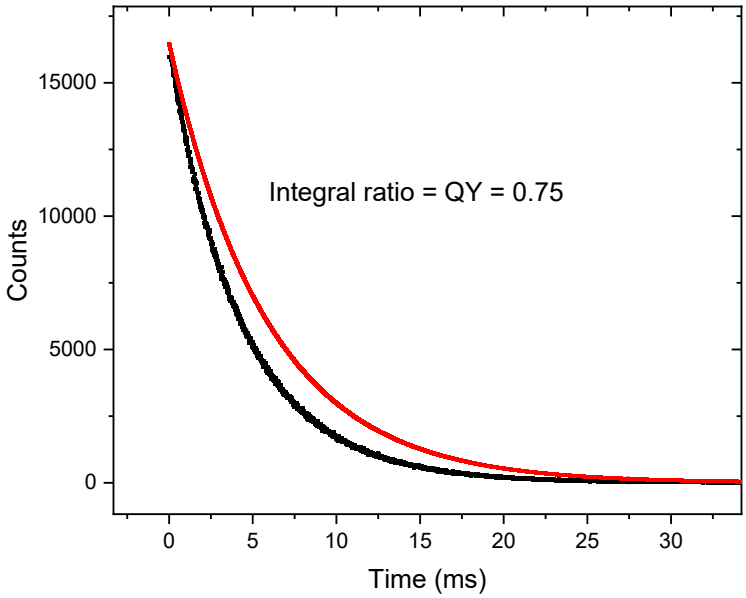

Figure S20. Decay curve (black line) of 592 nm Eu^{3+} emission for $LaPO_4:Eu^{3+}$ 5 at.% NPs in heptanol excited at 251 nm, and the radiative decay curve with QY = 1 (red line), τ_r = 5.86 ms.

S14. Global comparison of results

Table S10. Summary of ranges of parameters for $LaPO_4:Eu^{3+}$ 5 at.% NPs in different media

System	Type	RI range	$\tau(^5D_0)$ ms	*R*2	ED:MD	λ_{exc} (nm)
Bare NP		1.79	3.74(5)	0.98	3.53	251
Alcohols		1.38-1.42	4.09(8)-3.81(2) ¶	0.90-0.89	3.26(2)-3.23(2)	394
NP-glass mixture	P_2O_5-ZnO-PbO	1.58-1.87	3.5(2)-3.4(2) 3.4(1)-3.4(1) 3.4(1)-3.4(1)	1.2(3)-1.2(2)	2.6-2.7	394
	B_2O_3-TeO_2-Na_2O_3-CaO-TiO_2	2.42-2.58	3.57(4)-3.52(4) ¶ 3.5(1)-3.5(1)	1.35-1.34	3.78-3.78	394
	B_2O_3-BaO	1.56-1.64	3.91(4)-3.86(4) ¶ 3.88(7)-3.83(7)	0.95-0.94	3.12-3.15	251
Melted glass	B_2O_3-PbO-Eu_2O_3	1.68-2.06	2.1-1.1¶ 2.07(5)-1.07(2)	3.86-4.25	6.22-7.06	394
	B_2O_3-BaO-Eu_2O_3	1.58-1.64	3.01(0)-2.44(3) ¶ 2.9(2)-2.4(2)	3.57-4.74	5.80-7.38	394
	B_2O_3-TeO_2-Na_2O-CaO-TiO_2	2.42-2.58	2.09(3)-2.03(2) ¶ 2.0(1)-2.0(1)	5.68-5.41	8.56-8.30	394
Melted PiG	TeO_2–B_2O_3–ZnO–Na_2O–Al_2O_3	1.69	1.44 ¶ 1.39(8)	5.65	8.68	394
PiG	TeO_2–B_2O_3–ZnO–Na_2O–Al_2O_3	1.61-1.87	3.15(2)-3.24(8) ¶ 3.0(1)-2.3(2)	0.96(5)-1.9(3)	2.43(3)-3.6(2)	394
	TeO_2-ZnO-BaO	1.91-2.05	2.71(6)-2.48(3) ¶ 2.4(5)-2.3(4)	1.32-1.24	3.32-2.99	394
	TeO_2-B_2O_3-BaO	1.83-2.02	3.09(2)-2.87(4) ¶ 2.8(4)-2.6(3)	1.28-1.16	3.45-3.10	394

¶Neglecting the monitoring at 612 nm.

S15. References

1 K. Hickmann, K. Kömpe, A. Hepp and M. Haase, *Small*, 2008, **4**, 2136-2139.
2 Y. Luo, L. Li, H. T. Wong, K. L. Wong and P. A. Tanner, *Small*, 2020, **16**, 1905234.
3 M. A. Van De Haar, A. C. Berends, M. R. Krames, L. Chepyga, F. T. Rabouw and A. Meijerink, *J. Phys. Chem. Lett.*, 2020, **11**, 689-695.
4 Y. Kumar, S. Tripathi, M. Nand, R. Jangir, V. Srihari, A. Das, R. Singh, U. Deshpande, S. Jha and A. Arya, *J. Alloys Compds.*, 2022, **925**, 166772.
5 S. Fujino, H. Takebe and K. Morinaga, *J. Am. Ceram. Soc.*, 1995, **78**, 1179-1184.
6 A. Ali, Y. Rammah and M. Shaaban, *J. Non-Cryst. Solids*, 2019, **514**, 52-59.
7 H. Ticha, J. Schwarz, L. Tichy and R. Mertens, *J. Optoelectron. Adv. Mater.*, 2004, **6**, 747-754.
8 H. Chen, H. Lin, J. Xu, B. Wang, Z. Lin, J. Zhou and Y. Wang, *J. Mater. Chem. C*, 2015, **3**, 8080-8089.
9 J. Hrabovsky, F. Desevedavy, L. Strizik, G. Gadret, P. Kalenda, B. Frumarova, L. Benes, S. Slang, M. Veis and T. Wagner, *J. Non-Cryst. Solids*, 2022, **582**, 121445.
10 Y. Cha, J. Kim, J.-H. Yoon, B. Lee, S. Choi, K. Hong, E. Jeong, T. Komatsu and H. Kim, *J. Non-Cryst. Solids*, 2015, **429**, 143-147.
11 Y. Sun, Y. Wang, W. Chen, Q. Jiang, D. Chen, G. Dong and Z. Xia, *Nat. Commun.*, 2024, **15**, 1033.
12 Y. Yang, *Mater. Sci. Eng. B*, 2013, **178**, 807-810.
13 J. Dexpert-Ghys, R. Mauricot and M. Faucher, *J. Lumin.*, 1996, **69**, 203-215.
14 J. J. van Hest, G. A. Blab, H. C. Gerritsen, C. d. M. Donega and A. Meijerink, *Nanoscale Res. Lett.*, 2016, **11**, 261.
15 N. Niu, P. Yang, Y. Wang, W. Wang, F. He, S. Gai and D. Wang, *J. Alloys Compd*., 2011, **509**, 3096-3102.
16 T. Gavrilović, J. Periša, J. Papan, K. Vuković, K. Smits, D. J. Jovanović and M. D. Dramićanin, *J. Lumin.*, 2018, **195**, 420-429.
17 L. Yu, H. Song, S. Lu, Z. Liu, L. Yang and X. Kong, *J. Phys. Chem. B*, 2004, **108**, 16697-16702.
18 M. Runowski, T. Grzyb, A. Zep, P. Krzyczkowska, E. Gorecka, M. Giersig and S. Lis, *RSC Adv.*, 2014, **4**, 46305-46312.
19 D. Aspnes, *Am. J. Phys*, 1982, **50**, 704-709.
20 A. Souza, G. Cortes, H. Lima and M. C. dos Santos, *J. Lumin.*, 2019, **210**, 452-456.
21 A. S. Souza, J. L. Santos, H. Lima and M. C. dos Santos, *Physica B*, 2025, **703**, 416997.
22 C. Duan and M. Reid, *Spectrosc. Lett.*, 2007, **40**, 237-246.
23 C. Kittel, *Introduction to Solid State Physics*, Wiley: New York, 1976.
24 B. Henderson and G. F. Imbusch, *Optical spectroscopy of inorganic solids*, Oxford University Press, 2006.
25 D. Xiao, H.-Y. Kai, A. Huang, M. Song, K.-L. Wong and P. A. Tanner, *J. Lumin.*, 2024, **266**, 120322.
26 K. Binnemans, *Coord. Chem. Rev.*, 2015, **295**, 1-45.
27 K. Dolgaleva and R. W. Boyd, *Adv. Opt. Photon*., 2012, **4**, 1-77.

28 R. S. Meltzer, S. P. Feofilov, B. Tissue and H. Yuan, *Phys. Rev. B*, 1999, **60**, R14012.
29 T. T. Basiev, Y. V. Orlovskii and K. Pukhov, *Nanotechnol. Russia*, 2008, **3**, 551-559.
30 K. K. Pukhov, T. T. Basiev and Y. V. Orlovskii, *JETP Lett.*, 2008, **88**, 12-18.
31 K. K. Pukhov and T. T. Basiev, *Opt. Mater.*, 2010, **32**, 1664-1667.
32 M. E. Crenshaw and C. M. Bowden, *Phys. Rev. Lett.*, 2000, **85**, 1851.
33 M. E. Crenshaw, *Phys. Rev. A*, 2008, **78**, 053827.
34 P. Berman and P. Milonni, *Phys. Rev. Lett.*, 2004, **92**, 053601.
35 T. Senden, F. T. Rabouw and A. Meijerink, *ACS Nano*, 2015, **9**, 1801-1808.
36 J. J. van Hest, G. A. Blab, H. C. Gerritsen, C. de Mello Donega and A. Meijerink, *J. Phys. Chem. C*, 2017, **121**, 19373-19382.
37 E. Yablonovitch, T. Gmitter and R. Bhat, *Phys. Rev. Lett.*, 1988, **61**, 2546.
38 H. Chew, *Phys. Rev. A*, 1988, **38**, 3410.
39 C.-K. Duan, H. Wen and P. A. Tanner, *Phys. Rev. B*, 2011, **83**, 245123.